Research Article

Ni and Zn modified acid activated montmorillonite clay for effective removal of carbol fuchsin dye from aqueous solution

Sachin Girdhar Shinde[1] · Vinod Shankar Shrivastava[1]

Received: 8 September 2019 / Accepted: 18 February 2020

Abstract
The present work aims to investigate efficiency of zinc and nickel modified acid activated montmorillonite clay to remove carbol fuchsin dye from aqueous solution. The synthesized nanocomposites were characterized by TEM, SEM-EDAX, XRD, FT-IR and UV–Vis techniques. The adsorption of dye increased with increase in pH obeying pseudo-second-order rate kinetics and rapidly degraded (94%) alkaline dye solution in 90 min confirmed by LC–MS analysis. Zinc modified clay had slight edge due to high adsorption capacity and 3.24 eV band gap energy. Scavenger study confirmed participation of $O_2^{-\cdot}$ in degradation mechanism and reusability experiments confirmed stability of nanocomposites for multiple cycle.

Graphic abstract

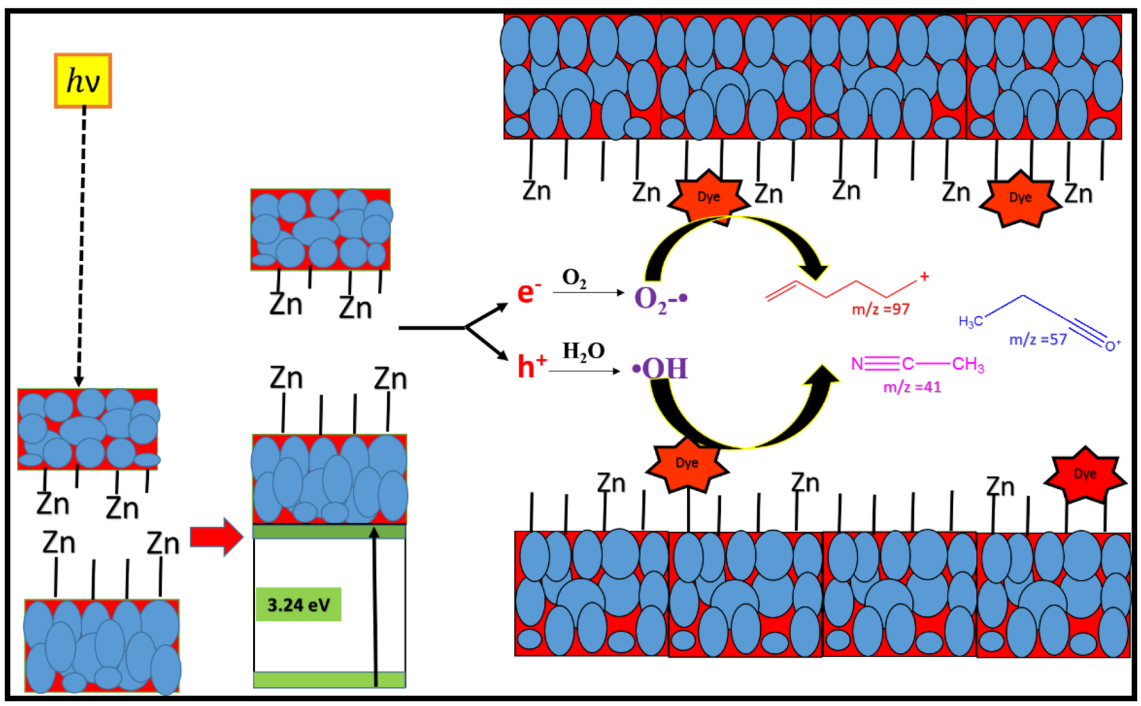

✉ Vinod Shankar Shrivastava, drvinodshrivastava1962@gmail.com | [1]Nanochemistry Research Laboratory, G.T.P. Arts, Commerce and Science College (Affiliated to Kavayitri Bahinabai Chaudhari North Maharashtra University, Jalgaon (MH), India), Nandurbar 425412, India.

SN Applied Sciences (2020) 2:519 | https://doi.org/10.1007/s42452-020-2295-1

Published online: 02 March 2020

Keywords Montmorillonite clay Nanocomposites · Carbol fuchsin · Photocatalytic degradation

1 Introduction

Over the last few decades due to the urbanization and industrialization, rapid increase in water pollution is observed due to the addition of large amount of organic matter in water bodies [1]. Various organic moieties such as pesticides, antibiotics, detergents and many others are introduced into the hydrosphere by urban waste and industrial effluents [1–3]. One of the major group of pollutants among all are organic dyes which are more than 100,000 types, manufactured at the rate of 10^5–10^6 tons per year and 10–15% of it goes as a waste through industrial effluent [4]. Many dyes when enter into the ecosystem prove lethal due to their aromatic origin, tendency to generate secondary metabolites carcinogens and absorption of essential sunlight in water bodies, Moreover, they increase BOD and COD by decreasing DO and can cause serious cytotoxic effects to aquatic life and eventually humans [4, 5]. To address the issue techniques such as coagulation, precipitation, filtration, oxidation, activated sludge processes, reverse osmosis, nano-filtration, ozone treatment and many more have been employed but possess limitations due to low efficiency, high cost and secondary waste product generation [6–8].

To tackle these limitations new techniques of Advanced Oxidation Processes (AOP's) are employed for complete destruction of organic pollutants in water bodies [9]. In these processes photo active materials are employed to generate highly oxidizing species such as $^{\cdot}OH$, $O_2^{-\cdot}$ for the degradation of organic molecules in presence of light known as photocatalysts [9, 10]. However, due to the high cost, less efficiency in UV–Vis range, toxicity and low reusability of these photocatalysts restrict the AOP's to be employed on large scale pilot projects [11, 12].

To overcome the drawbacks variety of naturally occurring, low cost clay minerals, such as montmorillonite clays [13], kaolinite clays [14], bentonite clays [15], activated clays [16] etc. can be effectively used as an adsorbent as well as photocatalysts. The efficiency of these materials can be increased by acid activation which increase the specific surface area, modify surface charges and adsorption capacity of clay minerals [16, 17] moreover, by incorporation of various metal dopants, which increase the catalytic ability by minimizing the band gap energy and modification of surface properties [18]. Zinc and nickel being highly photo active can be used as dopants to enhance the activity of clay minerals. Moreover, these dopants increase generation of photo induced charge carriers (e^-/h^+) and minimize their recombination, so they can effectively use to generate free radicals in aqueous solution [18, 19]. The peculiarities of activation and metal doping can be utilized to fabricate highly effective adsorbent and photocatalyst from low cost minerals by simple methods.

Considering the importance of low cost minerals, surface activation and incorporation of metal dopants herein, we report a large scale synthesis of zinc and nickel doped acid activated montmorillonite clay nanocomposites for efficient removal of rarely reported carbol fuchsin cationic dye under stimulated light source. Besides, effect of nickel and zinc incorporation is also investigated by comparing both the modified nanocomposite under various parameters.

2 Materials and methods

2.1 Materials

Montmorillonite clay was purchased from Rudra Zeolite, Nashik, India, Nickel (II) nitrate hexahydrate ($Ni(NO_3)_3{\cdot}6H_2O$), Zinc (II) nitrate hexahydrate ($Zn(NO_3)_3{\cdot}6H_2O$), Nitric acid (HNO_3) were purchased from Fisher Scientific, Carbol Fuchsin dye was purchased from SD Fine Chemical Limited, India, Polyethylene glycol—200 (PEG-200) (99.9%) and Sodium hydroxide (NaOH) were purchased from Merk, India.

2.2 Preparation of dye solution

Carbol fuchsin (CF) Fig. 1 was used as an organic contaminant. The stock solution (100 mg L^{-1}) of carbol fuchsin was prepared using double distilled water and various concentration of dye solutions were prepared by serial dilution from prepared stock solution.

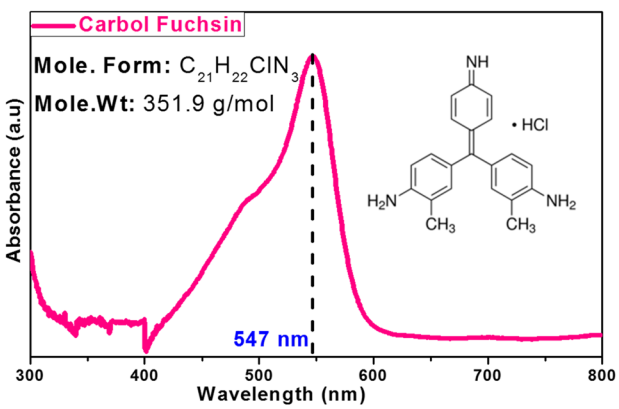

Fig. 1 Characteristics of carbol fuchsin (CF) dye

2.3 Activation of clay

For the acid activation 15 g of clay was grounded and sieved through 400 mesh filter cloth and continuously stirred in 250 ml of 0.25 M HNO_3 solution at 70 °C for 3 h. The resulting clay was filtered in Whatman-42 filter paper and washed several times with water to remove NO_3^- ions and resulting cake was dried in an open air oven at 110 °C for 4 h [20].

2.4 Synthesis of nickel and zinc modified acid activated Montmorillonite clay

After the acid activation, 10 g clay was dispersed in 300 ml, 0.5 M NaOH solution and stirred for 3 h at room temperature. 3 ml of PEG-200 was introduced and the mixture was further stirred for 1 h. Thereafter, 1 g each zinc nitrate/nickel nitrate precursors were separately added into the slurry and sonicated for 3 h with vigorous stirring. The resulting suspension was then filtered and the solid mass which separated out dried at 80 °C for 3 h. Then, the dry clay was calcined at 200 °C for 3 h in muffle furnace [21].

2.5 Characterization of nanocomposites

The synthesized clay composites were characterized by transmission electron microscopy (TEM) and X- ray diffraction (XRD) techniques to know the structure, phase composition and crystallinity of nanocomposites. The TEM analysis was carried out by Philips model CM 200. The morphology, porosity and elemental composition of clay composites was detected by the field–emission scanning electron microscopy (FESEM) and energy dispersive X- ray (EDAX) by model JSM 7600 F and fourier transform infrared spectroscopy (FT-IR) characterization was carried out by 3000 Hyperion Microscope with Vertex 800 FT-IR System, Bruker, Germany. The UV–Vis spectrum was recorded by Jasco V-730 double beam spectrophotometer.

3 Results and discussion

3.1 XRD analysis

The XRD patterns of synthesized nanocomposites are given in Fig. 2. The patterns resemble to a typical amorphous materials in which less distinct sharp peaks are appeared due to the presence of mixed crystalline phases of various metal oxides [22, 23]. The humps around 18.79° and 26.40° 2θ are originated due to the presence of Al_2O_3 and SiO_2 phases in the material confirmed the dominancy of aluminosilicate structure [24]. The peak at 35.06° 2θ corresponds to anatase TiO_2 and the peak at 42.06° 2θ is due

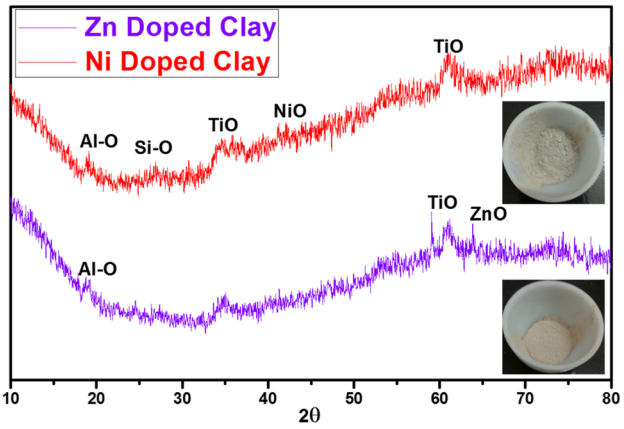

Fig. 2 XRD pattern of nickel and zinc doped acid activated montmorillonite clay

to the incorporation of nickel in the nickel doped nanocomposites [25]. Diffraction peak at 63.04° 2θ attributed to presence of zinc in the zinc modified clay nanocomposite [26]. The distortion in structural arrangement due to the acid activation leads to amorphous clay material in which small amount of crystallite structures are evident from the XRD pattern in both the synthesized nanocomposites [18].

3.2 TEM, SEM and EDAX analysis

The morphology, porosity and elemental composition of prepared nanocomposites were analyzed by SEM and EDAX characterization. The zinc incorporated acid activated montmorillonite clay in Fig. 3a revels heterogeneous clay morphology, clusters of clay particles and non-clay materials like oxides of sodium, potassium, calcium, magnesium etc. appear much more brighter (white) than the clay particles [20]. The elemental composition (Fig. 3c) of zinc modified clay comprised carbon which is incorporated due to the addition of PEG-200 during synthesis process is 14.09 %w. Si; 21.14 %w and Al; 5.33 %w respectively confirm the montmorillonite origin of synthesized nanocomposite [13]. One gram addition of zinc nitrate incorporated 0.83 %w of zinc into the clay nanocomposite. Remaining constituents are summarized in Fig. 3d. In nickel modified clay (Fig. 4a) the structure of nanocomposite is similar to the zinc modified clay in which 0.32 %w nickel is evident due to the addition of one gram of nickel nitrate and the elemental composition is given in Fig. 4d almost resembles to zinc modified nanocomposite.

TEM analysis of both the materials was carried out to know structural properties of nanocomposites. The heterogeneous crystallite nature of nanocomposites is confirmed in TEM images. Figures 3b and 4b of both the clay composites reveled hexagonal, ellipsoid, rod like structures of various metal oxides which are attached and encapsulated

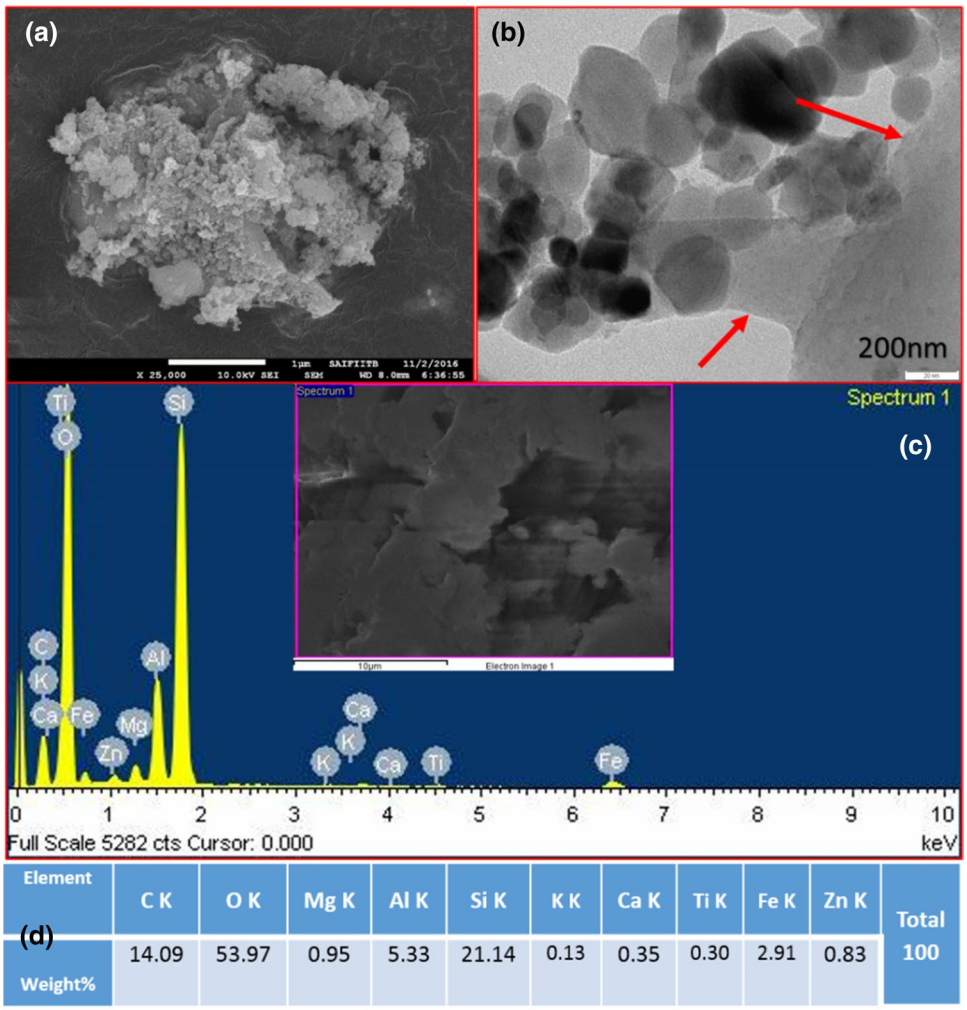

(d)

Element	C K	O K	Mg K	Al K	Si K	K K	Ca K	Ti K	Fe K	Zn K	Total
Weight%	14.09	53.97	0.95	5.33	21.14	0.13	0.35	0.30	2.91	0.83	100

Fig. 3 **a** SEM, **b** TEM, **c** and **d** EDAX characterization of zinc doped acid activated Montmorillonite clay

by parent clay layer (shown by red arrows), the enclosing is especially evident in zinc modified nanocomposite (Fig. 4b) [27, 28]. This confirms the heterogeneous morphology and variety of particle sized crystals incapsuled by clay minerals in both synthesized nanocomposites.

3.3 FT-IR analysis

FT-IR spectroscopy reveals chemical bonding information in a synthesized material and it was recorded in the range of 4000–400 cm^{-1}. Figure 5 shows the FT-IR transmittance spectra of both the modified clays. The presence of O–H stretching and H–O–H bending frequencies in the nanocomposites is evident from the peaks around 3625 cm^{-1} and 1638 cm^{-1} [29]. The characteristic clay frequencies due to the Si–O stretching attributed to 1042 cm^{-1} and 797 cm^{-1} respectively with the bands at 542 cm^{-1} and 468 cm^{-1} corresponding to deformation vibrations of Si–O–Al and Si–O–Si respectively [30]. The peaks around 530 cm^{-1} to 505 cm^{-1} corresponds to Zn–O and band in the region of 668 cm^{-1} confirms the presence of Ni–O in the synthesized nanocomposites [31, 32].

3.4 Optical property

The UV–Vis DRS spectra of both the materials were recorded and given in Fig. 6. The crystallite size, morphology and structural defects affect the band gap of nanocomposites. Both the modified clay show almost similar absorption maxima in the range of 335 nm which is less than unmodified montmorillonite system (365 nm) reported elsewhere [33]. This hypsochromic (blue) shift in absorption eventually affected the band gap energies in both the materials. The band gap energies of the materials were calculated by Tauc's method (Fig. 6 Inset) by following Eq. 1.

$$(\alpha hv) = C(hv - Eg) \quad (1)$$

where α is the absorption coefficient, *C* is constant, hv photon energy and Eg is the band gap. The plot of $(\alpha hv)^2$

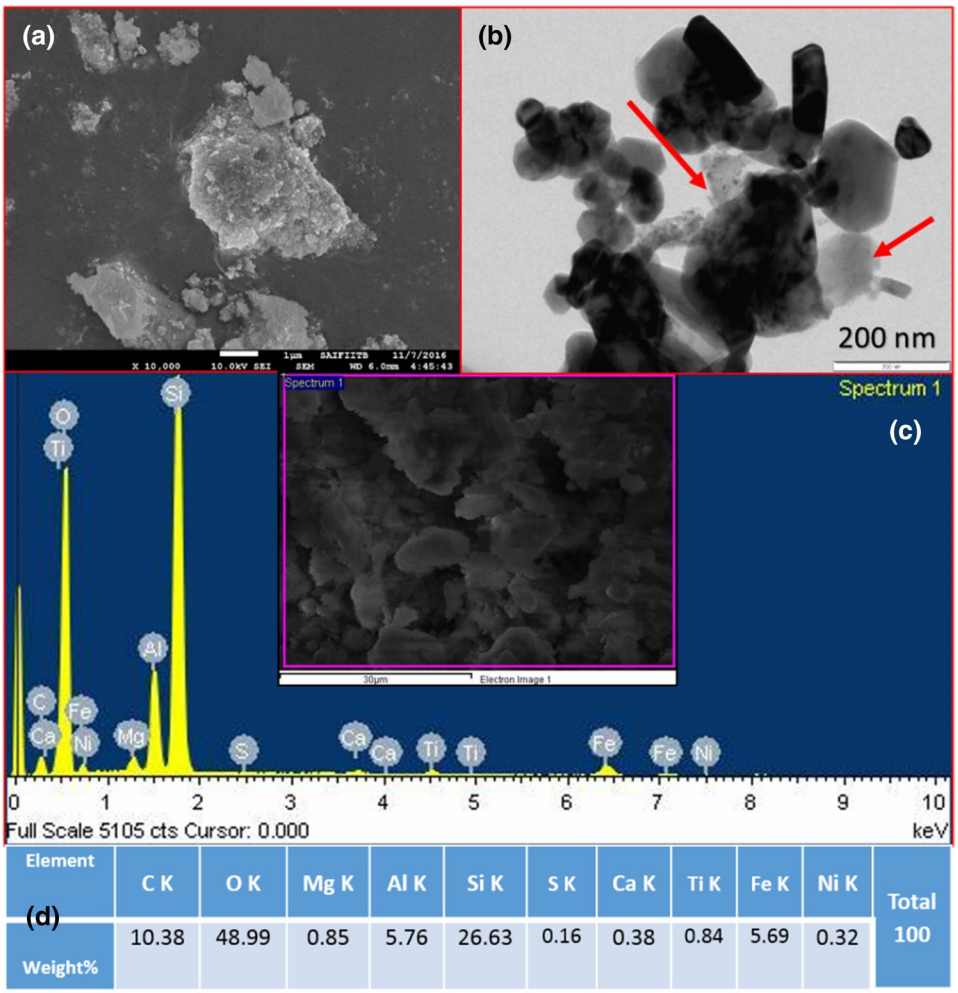

(d)

Element	C K	O K	Mg K	Al K	Si K	S K	Ca K	Ti K	Fe K	Ni K	Total
Weight%	10.38	48.99	0.85	5.76	26.63	0.16	0.38	0.84	5.69	0.32	100

Fig. 4 **a** SEM, **b** TEM, **c** and **d** EDAX characterization of nickel doped acid activated Montmorillonite clay

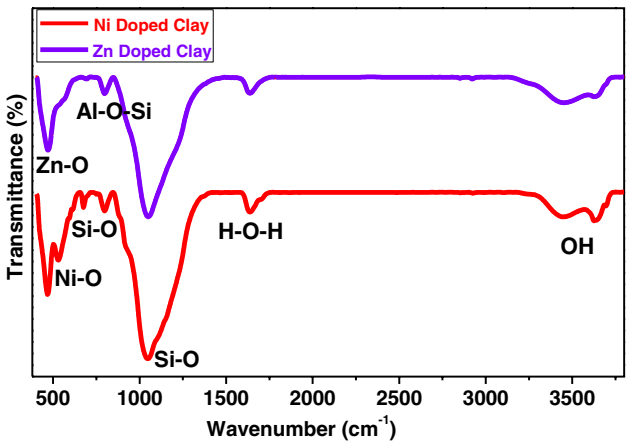

Fig. 5 FT-IR spectrum of nickel and zinc doped acid activated montmorillonite clay

versus hv was utilized to calculate the band gap energies [34]. It was found 3.24 eV for Zn and 3.29 eV for Ni modified nanocomposites respectively.

3.5 Adsorption studies

The effect of contact time on adsorption of carbol fuchsin (CF) dye by both the nanocomposites is given in Fig. 7. The parameters were optimized before the experiment in which the amount of catalyst was varied from 0.5 to 4.5 g L^{-1} and it was found that, after 1 g L^{-1} no appreciable increase of adsorption was observed may be due to the excess of catalyst. Similarly, pH was varied from 3 to 11.5 by 0.1 N HCl and 0.1 N NaOH solutions and it was evident, as the pH value increased the adsorption also increased however, after pH 10 no striking change in adsorption capacity was observed hence, pH 10 was chosen as minimum pH for further study. The concentration of 50 ml, pH 10 dye solution is varied from 20 to 80 mg L^{-1} and 1 g of zinc and nickel modified nanocomposites were separately dispersed in CF dye solution. The rate of adsorption was found directly proportional to the initial dye concentration and it was rapid up to 20 min then attained equilibrium and steadily inclined so forth. This observation is attributed to the availability of active

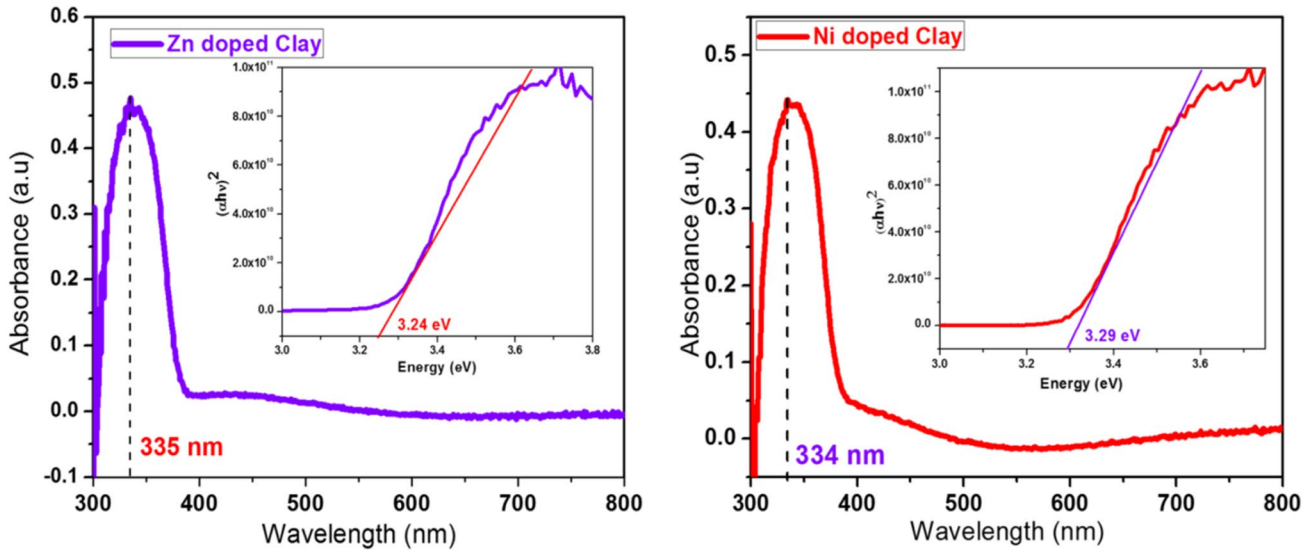

Fig. 6 Uv-Vis absorption spectrum and Tauc plots (inset) of nickel and zinc doped acid activated Montmorillonite clay

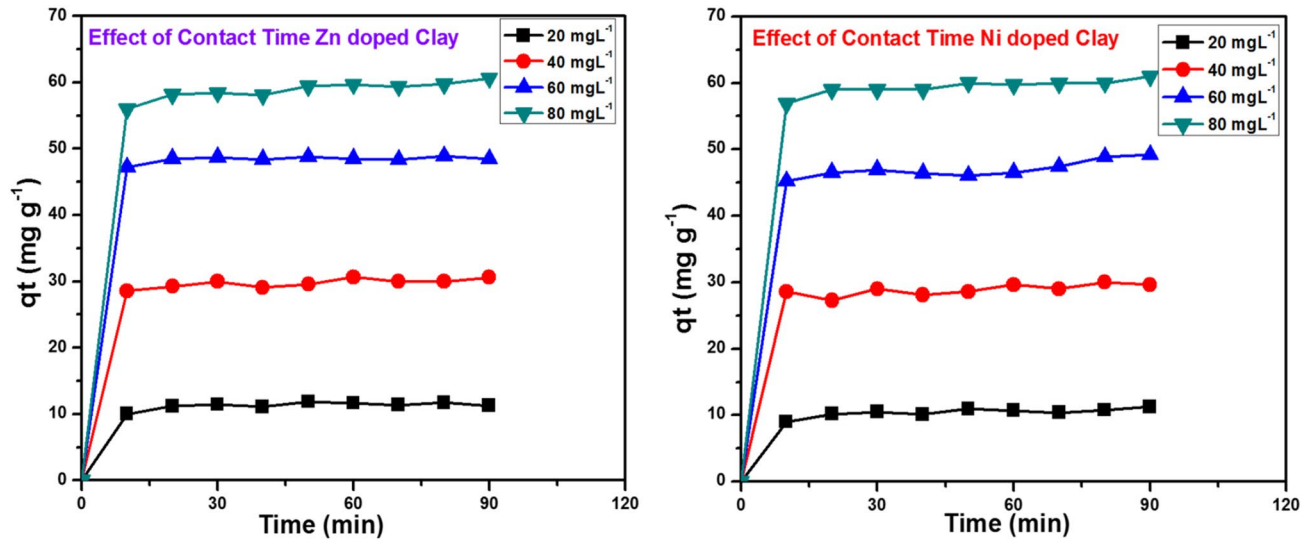

Fig. 7 Amount of dye adsorbed qt (mg g^{-1}) with time for different initial CF dye concentration (CF 50 mL, catalyst dose 1 g L^{-1}; pH 10)

sites for first 20 min and then repulsion due to the similar charges on the surface of nanocomposite and in bulk dye solution. The slight edge in adsorption capacity by zinc modified nanocomposite was observed when the zinc and nickel nanocomposites were separately dispersed in 20 mg L^{-1} of pH 10 CF dye solution (Fig. 7).

The adsorption kinetics was carried out to investigate the mechanism of adsorption (Fig. 8). The amount of CF adsorbed on both nanocomposites was calculated by Eq. 2.

$$qt = \frac{(C_o - C_t)V}{W} \quad (2)$$

where qt (mg g^{-1}) is the adsorption capacity at time t, C_o (mg L^{-1}) is the initial dye concentration; C_t (mg L^{-1}) is the dye concentration at time t, V (L) is the initial volume of dye solution and W (g) is the amount of nanocomposite. The pseudo-second-order model was used by plotting t/qt versus t [35] (Fig. 9). The amount of dye adsorbed qt increases from 10 to 60.3 mg g^{-1} as the initial dye

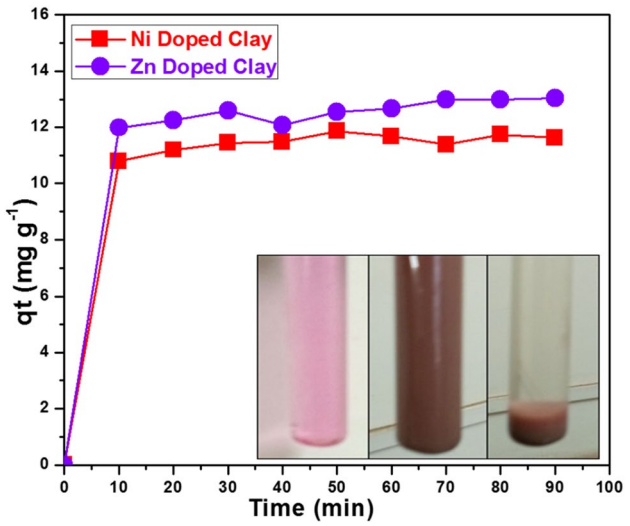

Fig. 8 Effect of contact time on adsorption of CF dye by doped clay nanocomposites (CF 50 mL 20 mg L^{-1} solution, catalyst dose 1 g L^{-1} and pH 10). Inset picture showing effective adsorption of alkaline dye solution by zinc doped nanocomposite

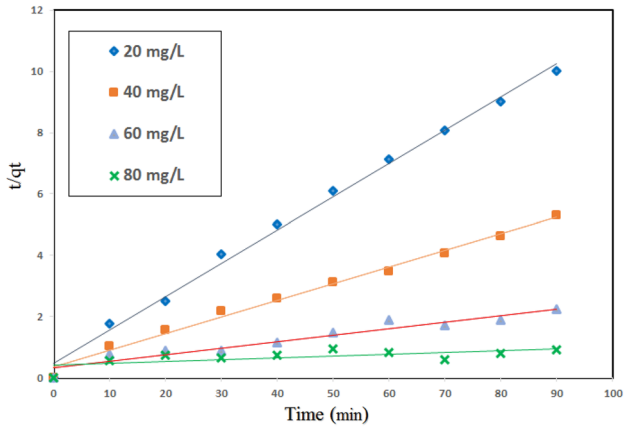

Fig. 9 Second order rate kinetics for the removal of CF at different initial concentration (zinc doped nanocomposite catalyst dose 1 g L^{-1}, pH 10)

concentration increased from 20 to 80 mg L^{-1} of 50 mL dye solution for 1 g L^{-1} adsorbent dose. The linear plot for 20 mg L^{-1} showed liner correlation coefficient (r^2) value 0.9943 confirmed the second-order rate kinetics [20].

3.6 Photocatalytic studies

The photocatalytic degradation of CF dye was carried out under stimulated UV–Vis irradiation using 400 W-mercury vapor lamp. The decolorization of CF dye was monitored by change in absorbance of 100 ml, 15 mg L^{-1} dye solution. 5 ml aliquots were withdrawn from the reaction assembly after 10 min of time interval, centrifuged and the supernatant solution was removed by pre cleaned syringe and subjected for the analysis in double beam spectrophotometer (Jasco V-730). The degradation percentages of CF were calculated by following Eq. 3. [15].

$$\text{Degradation} = \left(1 - \frac{C_t}{C_o}\right) \times 100 \quad (3)$$

where C_o is the concentration of CF before irradiation and C_t is the concentration after a certain irradiation time.

To optimize the reaction conditions effect of catalyst concentration and pH was studied by varying catalyst dose from 0.5 to 4.5 g L^{-1} and pH from 3 to 11.5. It was observed as the catalyst concentration increased the degradation efficiency also increased and the high efficiency was observed at 3 g L^{-1} thereafter, no appreciable change was observed due to light scattering by excess of catalyst in 100 ml dye solution [36]. The initial pH of the dye solution recorded was 8.3 and was varied by addition of 0.1 N HCl and 0.1 N NaOH solutions from 3 to 11.5. It was observed as the pH increased the degradation increased up to pH 10 thereafter, efficiency started to decrease may be due to the recombination of radical species and generation of radical scavenging CO_3^{2-} and HCO_3^- anions due to photogenerated and surrounding CO_2 [37]. By optimizing all the found parameter the photocatalytic efficiency of both the nanocomposites were separately investigated and it was found that zinc modified nanocomposite showed high catalytic efficiency up to 94% for 15 mg L^{-1} solution of CF dye within 90 min of irradiation time (Fig. 10a). The spectral variation during degradation of CF dye is given in Fig. 10b. The catalytic efficiency was found ~ 3.5% more than that of nickel nanocomposite. Furthermore, the zinc modified nanocomposite was subjected to multiple cycles to check the reusability. The catalyst was recovered by filtration and then dried at 150 °C for 2 h to eliminate adsorbed organic moieties [33]. It proved effective for multiple cycle and efficiency of forth cycle decreased by almost 8% as compared to first cycle (Fig. 11).

3.7 Photocatalytic mechanism and metabolite identification by LC–MS

To investigate the photocatalytic mechanism of CF dye degradation, isopropyl alcohol (IPA) and EDTA were used to trap $HO^{\cdot}$ and h^+ reactive species respectively. The number of h^+ generated are directly related to number of $O_2^{\cdot-}$ generation in an aqueous solution due to the generation of electrons (e^-) [38]. Keeping all the parameters constant and using 3 g L^{-1} of zinc modified nanocomposites the reaction assembly was placed under light (Fig. 12). Addition of 500 mM of IPA had very less effect on degradation

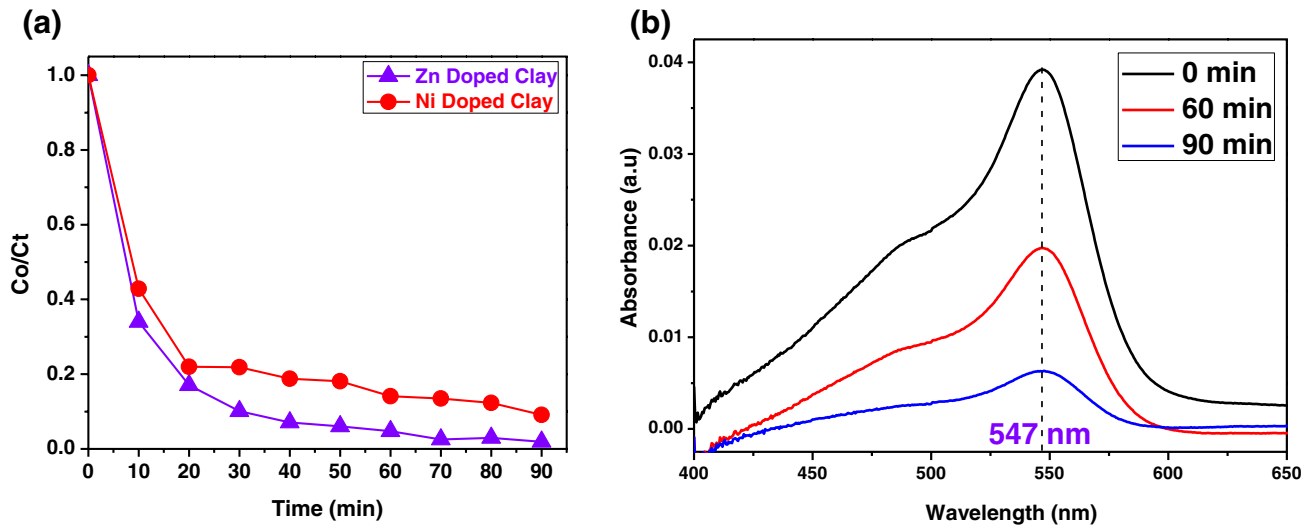

Fig. 10 **a** Photocatalytic degradation of CF dye by doped nanocomposites. (Catalyst dose 3 g L^{-1}, pH 10 and dye concentration 15 mg L^{-1}) **b** Spectral variations during CF degradation

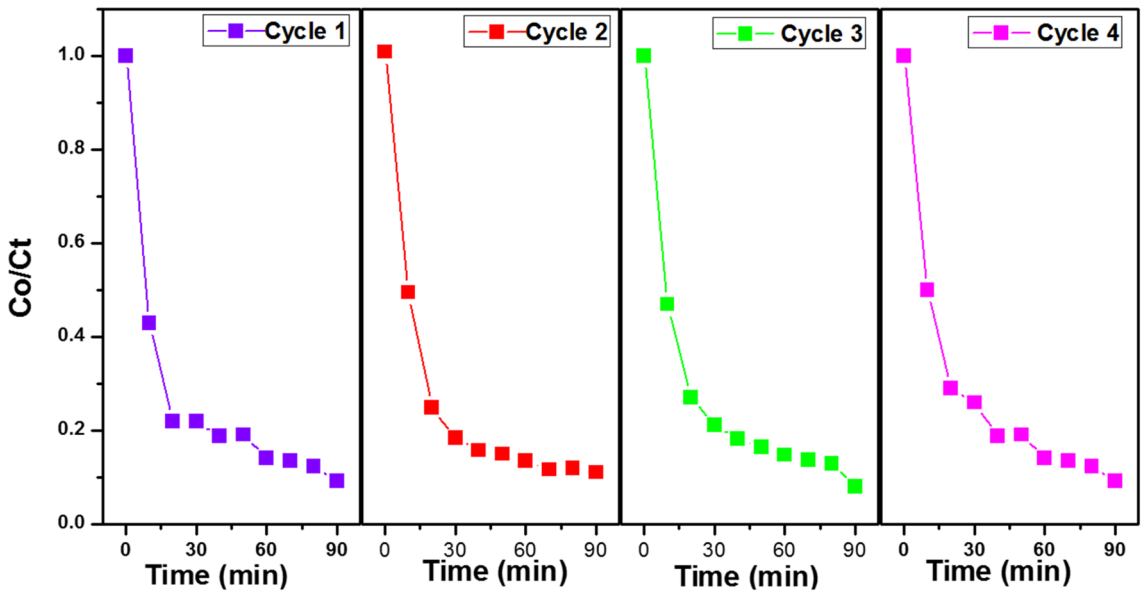

Fig. 11 Reusability of zinc doped acid activated Montmorillonite clay

capacity confirmed less participation of $HO^{\cdot}$. The photo generated electrons and h^{+} quencher EDTA almost stopped the degradation process and no further degradation was observed after adsorption, firmly established the participation $O_2^{\cdot-}$ in the degradation process [39].

The degradation of CF was also investigated by LC–MS technique (Fig. 13). Low molecular weight species were found in the LC–MS analysis of degraded dye solution confirmed complete degradation of large polycyclic dye molecule into its smaller and less harmful forms. This high oxidation attributed to the generation of highly reactive species due to higher pH of the dye solution [40]. The LC–MS spectra in Fig. 13 depicts high intense peak at 97, 57, and 41 m/z attributed to 1-hexene, propanal and acetonitrile molecular fragments respectively [40, 41]. The higher molecular weight species with less intense peaks signal larger molecular fragment in the degraded dye solution. The oxidation of aromatic amines in polycyclic dye molecule generated these types of smaller species due to Photo Klobe reaction carried out by free radical intermediates in aqueous solution [42].

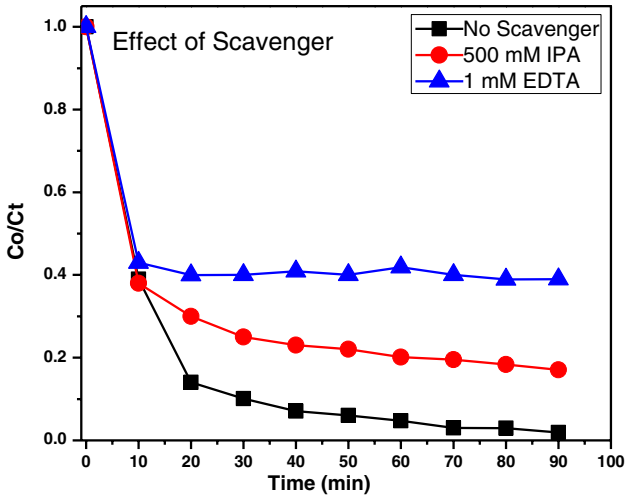

Fig. 12 Effect of scavengers on photocatalytic degradation of CF dye by zinc doped acid activated Montmorillonite clay (pH 10, concentration 15 mg L^{-1}, catalyst dose 3 g L^{-1})

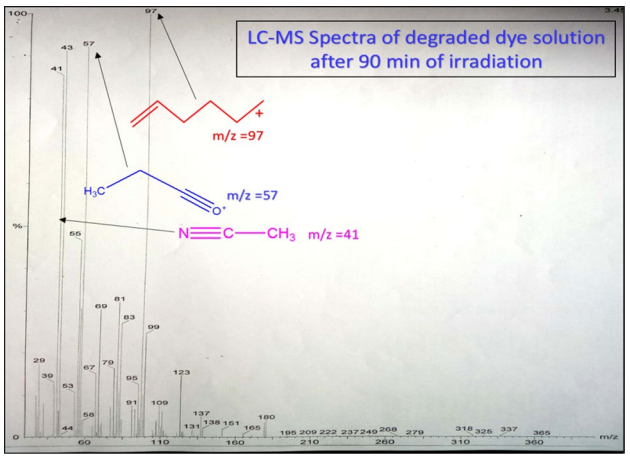

Fig. 13 LC–MS analysis of degraded CF dye solution after 90 min of irradiation

3.8 Comparative study of few low cost adsorbents

Low cost adsorbents are extensively used for the removal of organic as well as inorganic pollutants [43]. Here, only montmorillonite and modified types of montmorillonite clays are chosen for the comparative study specifically for the removal of organic contaminants from aqueous solution. Table 1 depicts few unmodified and modified montmorillonite type of low cost adsorbent in which pH, catalyst loading and maximum adsorption capacity of adsorbent is considered.

4 Conclusions

In summary, transition metal modified acid activated montmorillonite clay nanocomposite adsorbent as well as photocatalysts were synthesized and utilized for the effective adsorptive-degradation of CF cationic dye. The incorporation of zinc and nickel into the clay mineral confirmed by various characterization techniques. The zinc modified nanocomposite proved most efficient with respect to adsorption as well as degradation of organic contaminant up to 94%. The pseudo-second-order rate kinetics was confirmed and degradation took place at higher pH. The scavenger study confirmed the major participation of $O_2^{-\cdot}$ radical in degradation process and destructive degradation efficiency was confirmed by LC–MS study of degraded dye sample. Furthermore, high reusability up to four catalytic cycles was confirmed the synthesized materials are highly efficient, low cost photocatalyst for organic pollutant removal. In conclusion, the synthesized material is easy to synthesize and of low cost which makes it suitable both, as an adsorbent and photocatalyst. The adsorption separately can remove the pollutant makes it efficient material for large scale adsorption processes. The photocatalytic activity of the material can be enhanced by

Table 1 Comparative study of montmorillonite type of adsorbent for organic moieties removal

Sr. no.	Type of adsorbent	Contaminant	Adsorbent dose and optimum pH	Maximum adsorption capacity	References
1.	Sodium Montmorillonite Clay	Rhodamine B	0.3 g L^{-1}, pH = 7	42.19 mg g^{-1}	[44]
2.	Montmorillonite Clay	Methylene blue	3 g L^{-1}, pH = 11	300.30 mg g^{-1}	[45]
3.	Montmorillonite Clay	Fast green and malachite green dyes	1 gL^{-1}, pH = -	38.21 mg g^{-1}	[46]
4.	Chitosan/Modified Montmorillonite Beads	Reactive red 120	1 gL^{-1}, pH = 5	5.6085 mg g^{-1} (Monolayer)	[47]
5.	Montmorillonite Clay in Alginate Gel Beads	Polychlorinated biphenyls	0.1 g L^{-1}, pH = 5.5	2.45 µg g^{-1}	[48]
6.	Montmorillonite Clay	Malachite green	g L^{-1}, pH = 11	262.494 mg g^{-1}	[49]
7.	Zinc Doped Acid Activated Montmorillonite Clay	Carbol fuchsin	1 g L^{-1}, pH = 10	60.3 mg g^{-1}	This work

adding efficient metal dopants open the prospect for more active photocatalyst in near future.

Acknowledgements The research leading to these results has received support from IIT Bombay for FT-IR, EDAX, SEM, TEM characterization, K B C North Maharashtra University, Jalgaon for XRD Characterization and SICRT, SPPU, Pune for LC–MS analysis. Authors are also thankful to the Principal, G.T.P. College, Nandurbar and K. V. N. Naik A, C and S College, Nashik for providing necessary laboratory facilities.

Compliance with ethical standards

Conflict of interest The authors declare that there is no conflict of interests regarding the publication of this paper.

References

1. Petrie B, Barden R, Kasprzyk-Hordern B (2015) A review on emerging contaminants in wastewaters and the environment: current knowledge, understudied areas and recommendations for future monitoring. Water Res 72:3–27. https://doi.org/10.1016/j.watres.2014.08.053
2. Zhang LZ, Hong HS, Zhou JL, Huang J, Yu G (2003) Fate and assessment of persistent organic pollutants in water and sediment from Minjiang River Estuary, Southeast China. Chemosphere 52:1423–1430. https://doi.org/10.1016/S0045-6535(03)00478-8
3. Doll TE, Frimmel FH (2005) Removal of selected persistent organic pollutants by heterogeneous photocatalysis in water. Catal Today 101:195–202. https://doi.org/10.1016/j.cattod.2005.03.005
4. Pavithra KG, Kumar PS, Jaikumar V, Rajan PS (2019) Removal of colorants from wastewater: a review on sources and treatment strategies. J Ind Eng Chem 75:1–19. https://doi.org/10.1016/j.jiec.2019.02.011
5. Swati SS, Faruqui AN (2018) Investigation on ecological parameters and COD minimization of textile effluent generated after dyeing with mono and bi-functional reactive dyes. Environ Technol Innov 11:165–173. https://doi.org/10.1016/j.eti.2018.06.003
6. Gogate PR, Pandit AB (2004) A review of imperative technologies for wastewater treatment II:hybrid methods. Adv Environ Res 8:553–597. https://doi.org/10.1016/S1093-0191(03)00031-5
7. Lee CS, Robinson J, Chong MF (2014) A review on application of flocculants in wastewater treatment. Process Saf Environ Prot 92(6):489–508. https://doi.org/10.1016/j.psep.2014.04.010
8. Robinson T, McMullan G, Marchant R, Nigam P (2001) Remediation of dyes in textile effluent: a critical review on current treatment technologies with a proposed alternative. Bioresour Technol 77:247–255. https://doi.org/10.1016/S0960-8524(00)00080-8
9. An T, Yang H, Li G, Song W, Cooper WJ, Nie X (2010) Kinetics and mechanism of advanced oxidation processes (AOPs) in degradation of ciprofloxacin in water. Appl Catal B 94:288–294. https://doi.org/10.1016/j.apcatb.2009.12.002
10. Grebel JE, Pignatello JJ, Mitch WA (2010) Effect of halide ions and carbonates on organic contaminant degradation by hydroxyl radical-based advanced oxidation processes in saline waters. Environ Sci Technol 44:6822–6828. https://doi.org/10.1021/es1010225
11. Qi K, Cheng B, Yu J, Ho W (2017) Review on the improvement of the photocatalytic and antibacterial activities of ZnO. J Alloys Compd 727:792–820. https://doi.org/10.1016/j.jallcom.2017.08.142
12. Adnan MAM, Julkapli NM, Hamid SBA (2016) Review on ZnO hybrid photocatalyst: impact on photocatalytic activities of water pollutant degradation. Rev Inorg Chem 36(2):2–24. https://doi.org/10.1515/revic-2015-0015
13. Fatimah I, Wang S, Wulandari D (2011) ZnO/montmorillonite for photocatalytic and photochemical degradation of methylene blue. Appl Clay Sci 53:553–560. https://doi.org/10.1016/j.clay.2011.05.001
14. Chong MN, Vimonses V, Lei S, Jin B, Chow C, Saint C (2009) Synthesis and characterisation of novel titania impregnated kaolinite nano-photocatalyst. Microporous Mesoporous Mater 117:233–242. https://doi.org/10.1016/j.micromeso.2008.06.039
15. Sun Z, Chen Y, Ke Q, Yang Y, Yuan J (2002) Photocatalytic degradation of cationic azo dye by TiO_2/bentonite nanocomposite. J Photochem Photobiol A 149:169–174. https://doi.org/10.1016/S1010-6030(01)00649-9
16. Madejová J, Pálková H, Jankovi L (2015) Near-infrared study of the interaction of pyridine with acid-treated montmorillonite. Vib Spectrosc 76:22–30. https://doi.org/10.1016/j.vibspec.2014.11.003
17. He H, Guo J, Xie X, Lin H, Li L (2002) A microstructural study of acid-activated montmorillonite from Choushan. China Clay Miner 37:337–344. https://doi.org/10.1180/0009855023720037
18. Liu J, Zhang G (2014) Recent advances in synthesis and applications of clay-based photocatalysts: a review. Phys Chem Chem Phys 16:8178–8192. https://doi.org/10.1039/C3CP54146K
19. Espana VVA, Sarkar B, Biswas B, Rusmin R, Naidu R (2019) Environmental applications of thermally modified and acid activated clay minerals: current status of the art. Environ Technol Innov 13:383–397. https://doi.org/10.1016/j.eti.2016.11.005
20. Bhattacharyya KG, Gupta SS, Sarma GK (2015) Kinetics, equilibrium isotherms and thermodynamics of adsorption of Congo red onto natural and acid-treated kaolinite and montmorillonite. Desalin Wat Treat 53(2):530–542. https://doi.org/10.1080/19443994.2013.839405
21. Meshram S, Limaye R, Ghodke S, Nigam S, Sonawane S, Chikate R (2011) Continuous flow photocatalytic reactor using ZnO–bentonite nanocomposite for degradation of phenol. Chem Eng J 172:1008–1015. https://doi.org/10.1016/j.cej.2011.07.015
22. Liua H, Chaudharya D, Yusab S, Tadea MO (2011) Glycerol/starch/Na^+-montmorillonite nanocomposites: a XRD, FT-IR, DSC and ^1H NMR study. Carbo Poly 83:1591–1597. https://doi.org/10.1016/j.carbpol.2010.10.018
23. Li T, Zhang J, Xie X, Yin X, An X (2015) Montmorillonite-supported Ni nanoparticles for efficient hydrogen production from ethanol steam reforming. Fuel 143:55–62. https://doi.org/10.1016/j.fuel.2014.11.033
24. Kun R, Mogyorósi K, Dékány I (2006) Synthesis and structural and photocatalytic properties of TiO_2/montmorillonite nanocomposites. Appl Clay Sci 32:99–110. https://doi.org/10.1016/j.clay.2005.09.007
25. Clause O, Coelho MG, Gazzano M, Matteuzzi D, Trifirò F, Vaccari A (1993) Synthesis and thermal reactivity of nickel-containing anionic clays. Appl Clay Sci 8(2–3):169–186. https://doi.org/10.1016/0169-1317(93)90035-Y
26. Misra AJ, Das S, Rahman APH, Das B, Jayabalan R, Behera SK, Suar M, Tamhankar AJ, Mishra A, Lundborg CS, Tripathy SK (2018) Doped ZnO nanoparticles impregnated on Kaolinite (Clay): a reusable nanocomposite for photocatalytic disinfection of multidrug resistant Enterobacter sp. under visible light. J Colloid Interface Sci 530:610–623. https://doi.org/10.1016/j.jcis.2018.07.020
27. Belver C, Bedia J, Rodriguez JJ (2017) Zr-doped TiO_2 supported on delaminated clay materials for solar photocatalytic treatment

of emerging pollutants. J Hazard Mater 322:233–242. https://doi.org/10.1016/j.jhazmat.2016.02.028
28. Ghiassi S, Sedaghat S, Mokhtary M, Kefayati H (2018) Plant-mediated bio-synthesis of silver–montmorillonite nanocomposite and antibacterial effects on gram-positive and negative bacteria. J Nanostruct Chem 8:353–357. https://doi.org/10.1007/s40097-018-0280-7
29. Kongnoo A, Tontisirin S, Worathanakul P, Phalakornkule C (2017) Surface characteristics and CO_2 adsorption capacities of acid-activated zeolite 13X prepared from palm oil mill fly ash. Fuel 193:385–394. https://doi.org/10.1016/j.fuel.2016.12.087
30. Novakovic T, Rozic L, Petrovic S, Rosic A (2008) Synthesis and characterization of acid-activated Serbian smectite clays obtained by statistically designed experiments. Chem Eng J 137:436–442. https://doi.org/10.1016/j.cej.2007.06.003
31. Motshekga SC, Ray SS, Onyango MS, Momba MNB (2013) Microwave-assisted synthesis, characterization and antibacterial activity of Ag/ZnO nanoparticles supported bentonite clay. J Hazard Mater 262:439–446. https://doi.org/10.1016/j.jhazmat.2013.08.074
32. Mao H, Li B, Li X, Liu Z, Ma W (2009) Mesoporous nickel (or cobolt)-doped silica-pillared clay: synthesis and characterization studies. Mater Res Bull 44:1569–1575. https://doi.org/10.1016/j.materresbull.2009.02.002
33. Xu C, Gu FL, Wu H (2017) BiOCl-montmorillonite as a photocatalyst for highly efficient removal of Rhodamine B and Orange G: importance of the acidity and dissolved oxygen. Appl Clay Sci 147:28–35. https://doi.org/10.1016/j.clay.2017.07.025
34. Tauc J, Grigorovici R, Vancu A (1966) Optical properties and electronic structure of amorphous germanium. Phys Status Solidi 15(2):627–637. https://doi.org/10.1002/pssb.19660150224
35. Patil MR, Shrivastava VS (2015) Adsorption of malachite green by polyaniline–nickel ferrite magnetic nanocomposite: an isotherm and kinetic study. Appl Nanosci 5:809–816. https://doi.org/10.1007/s13204-014-0383-5
36. Kansal SK, Singh M, Sud D (2007) Studies on photodegradation of two commercial dyes in aqueous phase using different photocatalysts. J Hazard Mater 141:581–590. https://doi.org/10.1016/j.jhazmat.2006.07.035
37. Shinde SG, Patil MP, Kim G-D, Shrivastava VS (2019) Multi-doped ZnO photocatalyst for solar induced degradation of indigo carmine dye and as an antimicrobial agent. J Inorg Organome Polym Mater 2019:1–12. https://doi.org/10.1007/s10904-019-01273-2
38. Li M, Li X, Jiang G, He G (2015) Hierarchically macro–mesoporous ZrO_2–TiO_2 composites with enhanced photocatalytic activity. Ceram Int 41(4):5749–5757. https://doi.org/10.1016/j.ceramint.2014.12.161
39. Liu T, Wang L, Lu X, Fan J, Cai X, Gao B, Miao R, Wang J, Lv Y (2017) Comparative study of the photocatalytic performance for the degradation of different dyes by $ZnIn_2S_4$: adsorption, active species, and pathways. RSC Adv 7:12292–12300. https://doi.org/10.1039/c7ra00199a
40. Kang J, Price WE, Ashton J, Tapsell LC, Johnson S (2016) Identification and characterization of phenolic compounds in hydromethanolic extracts of sorghum wholegrains by LC-ESI-MS^n. Food Chem 211:215–226. https://doi.org/10.1016/j.foodchem.2016.05.052
41. Kolakowski BM, Grossert JS, Ramaley L (2004) Studies on the positive-ion mass spectra from atmospheric pressure chemical ionization of gases and solvents used in liquid chromatography and direct liquid injection. J Am Soc Mass Spectrom 15(3):311–324. https://doi.org/10.1016/j.jasms.2003.10.019
42. Yang D, Ni X, Chen W, Weng Z (2008) The observation of photo-Kolbe reaction as a novel pathway to initiate photocatalytic polymerization over oxide semiconductor nanoparticles. J Photochem Photobiol A 195:323–329. https://doi.org/10.1016/j.jphotochem.2007.10.020
43. Shahadat Momina, Md, Isamil S (2018) Regeneration performance of clay-based adsorbents for the removal of industrial dyes: a review. RSC Adv 8:24571–24587. https://doi.org/10.1039/c8ra04290j
44. Selvam PP, Preethi S, Basakaralingam P, Thinakaran N, Sivasamy A, Sivanesan S (2008) Removal of rhodamine B from aqueous solution by adsorption onto sodium montmorillonite. J Hazard Mater 155:39–44. https://doi.org/10.1016/j.jhazmat.2007.11.025
45. Almeida CAP, Debacher NA, Downs AJ, Cotteta L, Mello CAD (2009) Removal of methylene blue from colored effluents by adsorption on montmorillonite clay. J Colloid Interface Sci 332:46–53. https://doi.org/10.1016/j.jcis.2008.12.012
46. Tahir H, Hammed U, Sultan Md, Jahanzeb Q (2010) Batch adsorption technique for the removal of malachite green and fast green dyes by using montmorillonite clay as adsorbent. Afr J Biotechnol 9(48):8206–8214. https://doi.org/10.5897/AJB10.911
47. Kittinaovarat S, Kansomwan P, Jiratumnukul N (2010) Chitosan/modified montmorillonite beads and adsorption Reactive Red 120. Appl Clay Sci 48:87–91. https://doi.org/10.1016/j.clay.2009.12.017
48. Barreca S, Orecchio S, Pace A (2014) The effect of montmorillonite clay in alginate gel beads for polychlorinated biphenyl adsorption: isothermal and kinetic studies. Appl Clay Sci 99:220–228. https://doi.org/10.1016/j.clay.2014.06.037
49. Baybars AF (2015) Isotherm, kinetic and thermodynamic studies on the adsorption behavior of malachite green dye onto montmorillonite clay. Part Sci Technol 1(34):118–126. https://doi.org/10.1080/02726351.2015.1052122